Spoof plasmon analogue of metal-insulator-metal waveguides

Mikhail A. Kats,* David Woolf, Romain Blanchard, Nanfang Yu, and Federico Capasso

School of Engineering and Applied Sciences, Harvard University, 9 Oxford Street, Cambridge, Massachusetts 02138, USA

mikhail@seas.harvard.edu

Abstract: We describe the properties of guided modes in metallic parallel plate structures with subwavelength corrugation on the surfaces of both conductors, which we refer to as spoof-insulator-spoof (SIS) waveguides, in close analogy to metal-insulator-metal (MIM) waveguides in plasmonics. A dispersion relation for SIS waveguides is derived, and the modes are shown to arise from the coupling of conventional waveguide modes with the localized modes of the grooves in the SIS structure. SIS waveguides have numerous design parameters and can be engineered to guide modes with very low group velocities and adiabatically convert light between conventional photonic modes and plasmonic ones.

OCIS codes: (250.5403) Plasmonics; (160.3918) Metamaterials; (230.7370) Waveguides.

References and links

1. E. N. Economou, "Surface plasmons in thin films," Phys. Rev. **182**(2), 539–554 (1969).
2. H. Raether, *Surface Plasmons on Smooth and Rough Surfaces and On Gratings* (Springer, 1988).
3. S. A. Maier, "Plasmonics: fundamentals and applications" (Springer-Verlag, New York, 2007)
4. J. Zenneck, "Uber die Fortpflanzung ebener elektromagnetischer Wellen langs einer ebenen Leiterflache und ihre Beziehung zur drahtlosen Telegraphie," Ann. Phys. **328**(10), 846– (1907).
5. A. Sommerfeld, "Uber die Ausbreitung der Wellen in der drahtlosen Telegraphie," Ann. Phys. **333**(4), 665–736 (1909).
6. M. Osawa, "Surface-enhanced infrared absorption," in *Topics in Applied Physics* (Springer, 2001) vol. 81.
7. C. C. Chang, Y. D. Sharma, Y. S. Kim, J. A. Bur, R. V. Shenoi, S. Krishna, D. H. Huang, and S. Y. Lin, "A surface plasmon enhanced infrared photodetector based on InAs quantum dots," Nano Lett. **10**(5), 1704–1709 (2010).
8. K. Y. Xu, X. F. Lu, A. M. Song, and G. Wang, "Enhanced terahertz detection by localized surface plasma oscillations in a nanoscale unipolar diode," J. Appl. Phys. **103**(11), 113708 (2008).
9. J. A. Deibel, K. L. Wang, M. D. Escarra, and D. M. Mittleman, "Enhanced coupling of terahertz radiation to cylindrical wire waveguides," Opt. Express **14**(1), 279–290 (2006).
10. N. Yu, Q. J. Wang, M. A. Kats, J. A. Fan, S. P. Khanna, L. Li, A. G. Davies, E. H. Linfield, and F. Capasso, "Designer spoof surface plasmon structures collimate terahertz laser beams," Nat. Mater. **9**(9), 730–735 (2010).
11. G. Goubau, "Surface waves and their application to transmission lines," J. Appl. Phys. **21**(11), 1119 (1950).
12. W. Rotman, "A study of single-surface corrugated guides," Proc. of the IRE 39, 8 (1951).
13. J. B. Pendry, L. Martin-Moreno, and F. J. Garcia-Vidal, "Mimicking surface plasmons with structured surfaces," Science **305**(5685), 847–848 (2004).
14. F. J. Garcia-Vidal, L. Martin-Moreno, and J. B. Pendry, "Surfaces with holes in them: new plastomic metamaterials," J. Opt. A **7**, S97–S101 (2005).
15. S. A. Maier, S. R. Andrews, L. Martin-Moreno, and F. J. Garcia-Vidal, "Terahertz surface plasmon-polariton propagation and focusing on periodically corrugated metal wires," Phys. Rev. Lett. **97**(17), 176805 (2006).
16. C. R. Williams, S. R. Andrews, S. A. Maier, A. I. Fernandez-Dominguez, L. Martin-Moreno, and F. J. Garcia-Vidal, "Highly confined guiding of terahertz surface plasmon polaritons on structured metal surfaces," Nat. Photonics **2**(3), 175–179 (2008).
17. T. Okamoto, J. Simonen, and S. Kawata, "Plasmonic band gaps of structured metallic thin films evaluated for a surface plasmon laser using the coupled-wave approach," Phys. Rev. B **77**(11), 115425 (2008).
18. K. Song and P. Mazumder, "Active terahertz spoof surface plasmon polariton switch comprising the perfect conductor metamaterial," IEEE Trans. Electron. Dev. **56**(11), 2792 (2009).
19. B. Wang, Y. Jin, and S. He, "Design of subwavelength corrugated metal waveguides for slow waves at terahertz frequencies," Appl. Opt. **47**(21), 3694–3700 (2008).
20. J. Zhang, L. Cai, W. Bai, Y. Xu, and G. Song, "Slow light at terahertz frequencies in surface plasmon polariton assisted grating waveguide," J. Appl. Phys. **106**(10), 103715 (2009).

#147908 - $15.00 USD Received 23 May 2011; revised 25 Jun 2011; accepted 26 Jun 2011; published 18 Jul 2011

21. A. I. Fernández-Domínguez, E. Moreno, L. Martin-Moreno, and J. F. Garcia-Vidal, "Guiding terahertz waves along subwavelength channels," Phys. Rev. B **79**(23), 233104 (2009).
22. K. R. Welford and J. R. Sambles, "Coupled surface plasmons in a symmetric system," J. Mod. Opt. **35**(9), 1467 (1988).
23. R. Zia, M. D. Selker, P. B. Catrysse, and M. L. Brongersma, "Geometries and materials for subwavelength surface plasmon modes," J. Opt. Soc. Am. A **21**(12), 2442 (2004).
24. J. A. Dionne, L. A. Sweatlock, H. A. Atwater, and A. Polman, "Plasmon slot waveguides: Towards chip-scale propagation with subwavelength-scale localization," Phys. Rev. B **73**(3), 035407 (2006).
25. B. E. A. Saleh and M. C. Teich, *Fundamentals of Photonics* (Wiley, 1991)
26. U. S. Inan and A. S. Inan, *Electromagnetic Waves* (Prentice Hall, 2000)
27. P. Yeh, *Optical Waves in Layered Media* (Wiley, 2005)
28. For example, the COMSOL Multiphysics RF module allows for PMC boundary conditions for electromagnetic simulations, in addition to the more common PEC, perfectly matched layer (PML), etc.
29. Y. Zhang, J. von Hagen, M. Younis, C. Fischer, and W. Wiesbeck, "Planar artificial magnetic conductors and patch antennas," IEEE Trans. Antenn. Propag. **31**, 10 (2003).
30. D. J. Kern, D. H. Werner, A. Monorchio, L. Lanuzza, and M. J. Wilhelm, "The design synthesis of multiband artificial magnetic conductors using high impedance frequency selective surfaces," IEEE Trans. Antenn. Propag. **53**(1), 8 (2005).
31. C. R. Brewitt-Taylor, "Limitation on the bandwidth of artificial perfect magnetic conductor surfaces," IET Microw. Antennas Propag. **1**(1), 255–260 (2007).
32. F. Gires and P. Tournois, "Interferometre utilisable pour la compression d'impulsions lumineuses modulees en frequence," C. R. Acad. Sci. Paris **258**, 6112 (1964).
33. A. D. Boardman, *Electromagnetic Surface Modes* (Wiley, 1982)
34. H. M. Barlow and A. L. Cullen, "Surface waves," Proc. of the Institution. of Electrical. Engineers. London. **100**, 68 (1953).
35. M. Cardona, "Fresnel Reflection and Surface Plasmons," Am. J. Phys. **39**(10), 1277 (1971).
36. The RF Module of COMSOL Multiphysics 4 was used to perform finite element calculations.
37. S. H. Mousavi, A. B. Khanikaev, B. Neuner 3rd, Y. Avitzour, D. Korobkin, G. Ferro, and G. Shvets, "Highly confined hybrid spoof surface plasmons in ultrathin metal-dielectric heterostructures," Phys. Rev. Lett. **105**(17), 176803 (2010).
38. X. Y. Miao, B. Passmore, A. Gin, W. Langston, S. Vangala, W. Goodhue, E. Shaner, and I. Brener, "Doping tunable resonance: toward electrically tunable mid-infrared metamaterials," Appl. Phys. Lett. **96**(10), 101111 (2010).
39. D. Woolf, M. Loncar, and F. Capasso, "The forces from coupled surface plasmon polaritons in planar waveguides," Opt. Express **17**(22), 19996–20011 (2009).
40. K. L. Tsakmakidis, A. D. Boardman, and O. Hess, "Trapped rainbow storage of light in metamaterials," Nature **450**(7168), 397–401 (2007).
41. H. Shin, M. F. Yanik, S. Fan, R. Zia, and M. L. Brongersma, "Omnidirectional resonance in a metal-dielectric-metal geometry," Appl. Phys. Lett. **84**, 22 (2004).
42. Q. Gan, Z. Fu, Y. J. Ding, and F. J. Bartoli, "Ultrawide-bandwidth slow-light system based on THz plasmonic graded metallic grating structures," Phys. Rev. Lett. **100**(25), 256803 (2008).
43. Q. Gan, Y. J. Ding, and F. J. Bartoli, "Rainbow trapping and releasing at telecommunication wavelengths," Phys. Rev. Lett. **102**(5), 056801 (2009).
44. A. Rusina, M. Durach, K. A. Nelson, and M. I. Stockman, "Nanoconcentration of terahertz radiation in plasmonic waveguides," Opt. Express **16**(23), 18576–18589 (2008).
45. M. J. Lockyear, A. P. Hibbins, and J. R. Sambles, "Microwave surface-plasmon-like modes on thin metamaterials," Phys. Rev. Lett. **102**(7), 073901 (2009).
46. M. Navarro-Cia, M. Beruete, S. Agrafiotis, F. Falcone, M. Sorolla, and S. A. Maier, "Broadband spoof plasmons and subwavelength electromagnetic energy confinement on ultrathin metafilms," Opt. Express **17**(20), 18184–18195 (2009).

1. Introduction

Surface plasmons (SPs) are electron oscillations on the surface of a metal at an interface with a dielectric that allow light to be confined and controlled at the subwavelength scale [1–3]. At infrared frequencies and below, the properties of metals approach those of a perfect electric conductor (PEC), and SPs become Zenneck or Sommerfeld waves which exhibit very poor confinement to the interface [4,5]. Therefore, an alternative method to confine and control fields at these frequencies is required to enable or improve a number of infrared (IR), terahertz (THz), and microwave applications such as surface-enhanced infrared absorption (SEIRA) spectroscopy [6], surface enhanced infrared photodetection [7], enhanced THz detection [8], outcoupling from photoconductive antennas [9], and THz laser beam-shaping [10].

Metallic surfaces with corrugations have been previously studied as guides for surface electromagnetic modes [11, 12], with the corrugation providing additional control over

#147908 - $15.00 USD Received 23 May 2011; revised 25 Jun 2011; accepted 26 Jun 2011; published 18 Jul 2011

electromagnetic fields. Recently, THz modes on subwavelength-corrugated conductors have been identified as 'spoof' surface plasmons (SSPs), which emulate optical frequency surface plasmons on flat metallic surfaces and enable the concentration of THz radiation at a metal/dielectric interface [13–16]. To date there have been a number of studies of SSPs on a single corrugated surface, but only limited analysis regarding coupled modes across multiple corrugated interfaces [17–21].

In this article, we analyze the guided modes of a parallel plate waveguide with subwavelength corrugations on both surfaces. These corrugations significantly alter the electromagnetic modes on both sides of the light line compared to both the non-corrugated parallel plate waveguide and the single corrugated interface. The geometrical parameters of the corrugations provide a large degree of control over dispersion properties and field distributions of light in such a waveguide. We analytically derive the dispersion relations of these modes and elucidate their unique properties. We identify several electromagnetic modes with flat dispersion and very low group velocity resulting from the coupling of SSPs, and then show that interaction between these new modes and the modes of a conventional parallel plate waveguide can result in large anti-crossing behavior in the dispersion curves. Because our structure is closely related to non-corrugated metal-insulator-metal (MIM) waveguides in plasmonics [22–24], we will refer to the doubly-corrugated geometry as a spoof-insulator-spoof (SIS) waveguide.

2. Theory of SIS Waveguides

Before discussing the modes and dispersion of an SIS waveguide, it is instructive to consider two well-studied metallic structures: the parallel plate waveguide and a single corrugated metallic surface. In both cases, as well as for the majority of this paper, we will assume that the metal is highly conductive at our frequency of interest and can be treated as a PEC.

The conventional parallel plate (or planar mirror) waveguide consists of two flat metallic surfaces separated by an air gap g (Fig. 1(a)). A textbook method of calculating the dispersion in this waveguide is to assume that a plane wave is propagating between the two parallel plates at some angle θ from the surface tangent and is reflected at each interface, imparting a ϕ phase shift in the electric field upon each reflection. By imposing a self-consistency condition that requires the phase fronts to reproduce themselves after two reflections (Fig. 1(a)), we obtain the mode dispersion [25]. This condition can be written as

$$\frac{4\pi g}{\lambda_0\sqrt{1+(k_x/k_z)^2}}+2\phi=2\pi m \qquad (1)$$

where $k_z=k_0\cos(\theta)$, $\beta=k_x=k_0\sin(\theta)$ is the propagation constant, m is an integer, and λ_0 and k_0 are the free space wavelength and wave vector, respectively.

For the case of reflection by a flat PEC at any angle of incidence, the phase of the reflected wave ϕ is always π, therefore the dispersion relation can be written as $\beta^2=k_0^{\,2}-(m^2\pi^2)/g^2$.

#147908 - $15.00 USD Received 23 May 2011; revised 25 Jun 2011; accepted 26 Jun 2011; published 18 Jul 2011

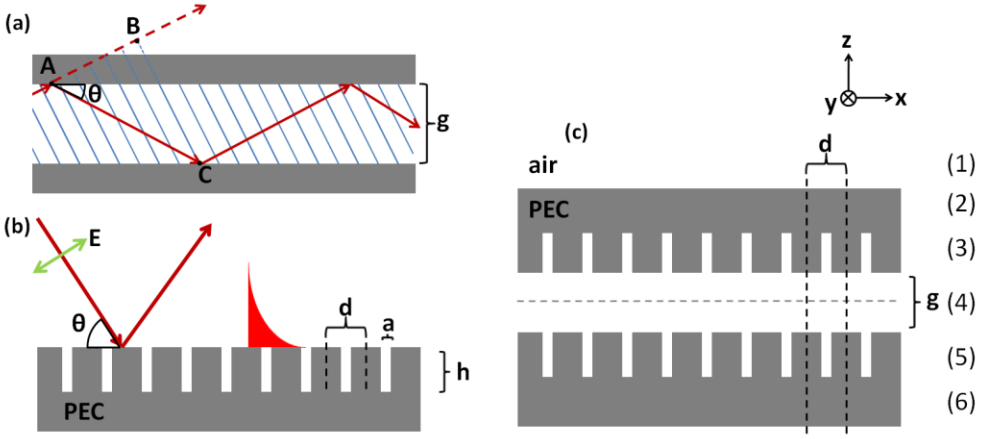

Fig. 1. (a.) Conventional parallel plate waveguide with the mode self-consistency condition illustrated (adapted from [24]). (b.) Periodically corrugated PEC surface with the unit cell identified by vertical dashed lines. If the corrugation is substantially subwavelength ($\lambda >> d$), this structure can support bound TM surface modes dubbed spoof surface plasmons (SSPs). (c.) Spoof-insulator-spoof (SIS) waveguide comprising two counter-facing structures from Fig. 1(b) separated by an air gap of height g. The numbers on the right identify the layers used in the transfer matrix calculations.

The case of propagating surface modes on a single corrugated metallic interface has been extensively analyzed in literature [11–14], and we re-derive the key points below. The system is illustrated in Fig. 1(b), and consists of a PEC bounded by air with a periodic corrugation of deeply-subwavelength grooves of width a, period d, and height h.

Each groove can be viewed as a truncated parallel plate waveguide in the z direction. Since the walls of this waveguide are perfectly conducting, there are no plasmonic modes in this geometry. Due to the deeply-subwavelength nature of the corrugation ($\lambda_0 >> d > a$), the only supported mode is the fundamental transverse magnetic (TM) mode for which only the y-component of the magnetic field and the x-component of the electric field are non-zero [26]. Since the electric field in this mode is also normal to the direction of propagation, it is referred to as a transverse electromagnetic (TEM) mode. Since there are no allowed modes with y- or z- polarization, the array of deeply-subwavelength grooves behaves as a PEC for y- or z-polarized light ($\epsilon_y = \epsilon_z = \infty$).

For light in the TEM mode of each groove, $k_z = k_0$ and $k_x = 0$, so the effective mode index is simply $n_{eff} = \sqrt{\epsilon_x \mu_y}$. In the limit of $\lambda_0 >> d$, the characteristic wave impedance η is simply the weighted average of the impedances of free space ($\eta = 1$) and a PEC ($\eta = 0$) based on the duty cycle of the structure, so $\eta = \sqrt{\mu_y / \epsilon_x} = a / d$.

This means that in the metamaterial limit, the structure of Fig. 1(b) can be treated as a homogeneous anisotropic layer of thickness h on the flat surface of a PEC, with the permittivity of the corrugated layer represented by a diagonal tensor $\overline{\overline{\epsilon}}_{spoof}$ with components $\epsilon_x = d / a$ and $\epsilon_y = \epsilon_z = \infty$ and the permeability represented by $\overline{\overline{\mu}}_{spoof}$ with components $\mu_y = \mu_z = 1/\epsilon_x$ and $\mu_x = 1$. The same result was previously obtained by rigorous mode-matching analysis by García-Vidal *et al.* [14].

Because the groove array functions as a PEC for y- or z-polarized light, the structure of Fig. 1(b) is equivalent to a flat PEC surface for all but TM polarized light and hence does not support any surface TE modes, so we will only be interested in identifying the TM modes which are significantly affected by the corrugation.

#147908 - $15.00 USD Received 23 May 2011; revised 25 Jun 2011; accepted 26 Jun 2011; published 18 Jul 2011

We calculate the TM electric field reflection coefficient r_c from the corrugated structure of Fig. 1(b) by treating it as a three layer system, with air on top, PEC on the bottom, and a homogeneous layer of height h in the middle with dielectric properties given by $\overline{\overline{\epsilon}}_{spoof}$ and $\overline{\overline{\mu}}_{spoof}$. The TM reflection and transmission coefficients for the electric field upon reflection or transmission from layer i to j are given by [26]

$$r_{ij} = \frac{k_{z,j}/\eta_i - k_{z,i}/\eta_j}{k_{z,j}/\eta_i + k_{z,i}/\eta_j} \tag{2i}$$

$$t_{ij} = \frac{2k_{z,j}/\eta_i}{k_{z,j}/\eta_i + k_{z,i}/\eta_j} \tag{2ii}$$

where $\eta_i = \sqrt{\mu_{y,i}/\epsilon_{x,i}}$ is the wave impedance, $\epsilon_{x,i}$ is the x-component of the permittivity, and $\mu_{y,i}$ is the y-component of the permeability in medium i. Here $k_{z,j}$ is the z-component of the wave vector in material j, and can be written as $k_{z,j} = \sqrt{k_0^2 \epsilon_{x,j}\mu_{y,j} - k_x^2}$. The value of r_{ij} is always -1 when medium j is a PEC, indicating complete reflection of energy with a π phase shift in the electric field.

To calculate r_c we apply the transfer matrix formalism [27], in which the 2 x 2 matrix D_{ij} describes the i - j interface and Φ_l describes the propagation through medium l.

$$D_{ij} = \frac{1}{t_{ij}}\begin{pmatrix} 1 & r_{ij} \\ r_{ij} & 1 \end{pmatrix} \tag{3i}$$

$$\Phi_l = \begin{pmatrix} e^{ik_{z,l}h} & 0 \\ 0 & e^{-ik_{z,l}h} \end{pmatrix} \tag{3ii}$$

The total transfer matrix to describe the three layer structure in Fig. 1(b) can then be written as $M = D_{12}\Phi_2 D_{23}$ where 1, 2, and 3 represent the air, the corrugation, and the continuous PEC layer, respectively. The reflection coefficient r_c can be obtained from M by $r_c = M_{2,1}/M_{1,1}$, where $M_{i,j}$ is the component of M identified by row i and column j, to yield

$$r_c = |r_c|e^{i\phi} = \frac{\left(\frac{d}{a}k_z - k_0\right) + \left(k_0 + \frac{d}{a}k_z\right)e^{2ik_0h}}{\left(\frac{d}{a}k_z + k_0\right) - \left(k_0 - \frac{d}{a}k_z\right)e^{2ik_0h}}. \tag{4}$$

In Eq. (4), k_z and k_x refer to the wave vector components in air (i.e. $k_z = k_{z,1}$ and $k_x = k_{x,1}$).

The phase of the reflected light ϕ is both a function of frequency and incidence angle $\theta = \tan^{-1}(k_z/k_x)$. Note that since the metal is a PEC and we assumed that the corrugation is deeply-subwavelength, there is no absorption and no diffracted orders other than specular reflection, so $|r_c| = 1$.

Since each groove is a parallel plate waveguide bounded by a PEC on one side and by air on the other, it can be viewed as a cavity in the vertical direction. As the mode in each groove is a TEM mode with $k = k_0$, we can write the resonance condition as $h = m\lambda_{0,m}/4$ or

#147908 - $15.00 USD Received 23 May 2011; revised 25 Jun 2011; accepted 26 Jun 2011; published 18 Jul 2011

$f_m = mc/4h$ where m is an odd positive integer. The field distributions for the first two cavity modes are illustrated in Fig. 2(a). Because the impedance of the corrugated layer is higher than that of a continuous PEC, yet lower than that of free space, there is an electric field node at the bottom of the cavity and an anti-node at the top.

It turns out that while the reflection phase ϕ is π for a flat PEC interface for all angles of incidence, in the corrugated PEC structure in Fig. 1(b) ϕ strongly deviates from π for frequencies which correspond to these localized cavity resonances. For a duty cycle $a/d = 0.1$, ϕ is plotted in Fig. 2(b) for several frequencies in the vicinity of the fundamental resonance frequency f_1 of the metallic groove cavity. Off resonance, ϕ approaches π for all but very small incidence angles (grazing incidence); however exactly on resonance, the ϕ is identically 0 for all θ. Around the resonant frequency, then, the corrugated interface acts as a perfect magnetic conductor (PMC). A PMC is like a PEC in that it reflects 100% of electromagnetic energy incident on it, but it does so with no reflection phase (ϕ = 0). Though no broadband PMC surfaces have ever been demonstrated, PMC boundary conditions are commonly used to simplify electromagnetic simulations [28], and a body of literature exists regarding artificial PMCs that achieve zero reflection phase over a narrow frequency range (see, for example [29–31],). The corrugated structure of Fig. 1(b) is one such artificial PMC. Note that the structure of Fig. 1(b) can also be viewed as a type of Gires-Tournois interterferometer, which is a classical optical element which reflects all of the light incident on it with a reflection phase that strongly depends on the wavelength of incident light [32].

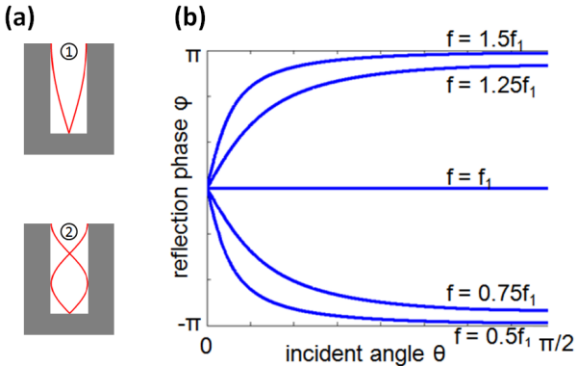

Fig. 2. (a.) Illustrated first and second order resonances of a groove cavity, with an electric field node at the bottom and an antinode at the opening. (b.) Reflection phase ϕ vs. incidence angle θ from a corrugated interface around the fundamental resonant frequency f_1 of the metallic grooves.

For all real incidence angles θ, $k_x \le k_0$. By relaxing this condition and allowing values of $k_x > k_0$, we are able to begin analyzing fields which are evanescent in the z direction $(k_z = i\sqrt{k_x^2 - k_0^2})$, corresponding to a complex θ. For either real or complex θ, the values at which the reflection coefficient r_c is undefined (i.e. the denominator of Eq. (4), $M_{1,1} = 0$) correspond to eigenmodes of the structure [33]. This approach has been used to analyze Zenneck waves and surface plasmons on finitely conducting metals where the divergence of r_c happens at the complex Brewster angle of incidence [34,35].

Thus, setting the denominator of Eq. (4) to zero leads to the dispersion relation of the surface modes of the structure of Fig. 1(b):

$$\beta^2 = \left(\frac{a}{d}\right)^2 k_0^2 \tan^2(k_0 h) + k_0^2, \tan(k_0 h) > 0 \qquad (5)$$

#147908 - $15.00 USD Received 23 May 2011; revised 25 Jun 2011; accepted 26 Jun 2011; published 18 Jul 2011

The dispersion relation of Eq. (5) is plotted as the black solid lines in Fig. 3(a) for h = 50μm along with the dispersion of the parallel plate waveguide of Fig. 1(a). Only the m = 0 (transverse-electromagnetic or TEM, blue) and m = 1 (TM1, red) modes exist in this range of frequencies in the parallel plate waveguide.

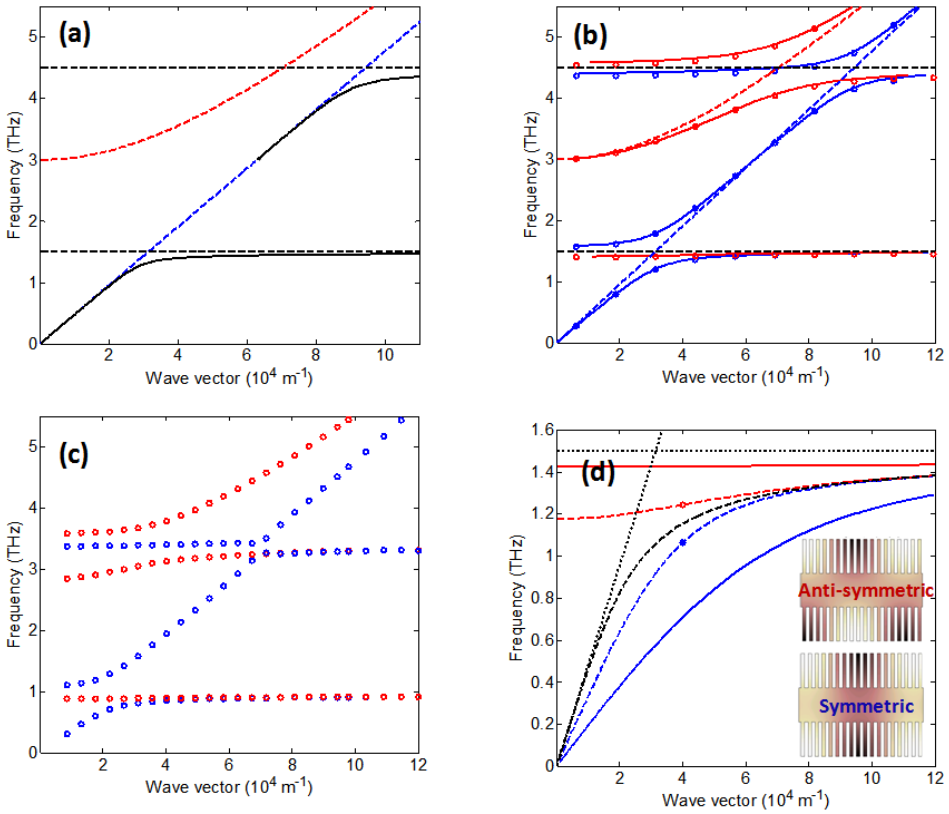

Fig. 3. (a.) Dispersion diagram of the parallel plate waveguide in Fig. 1(a) (red and blue lines) with g = 50μm, and of the single corrugated structure in Fig. 1(b) (solid black lines) with a = 1μm, d = 10μm, and h = 50μm. The red line is the dispersion of the fundamental TEM mode of the parallel plate waveguide, which is symmetric, while the blue line represents the antisymmetric TM1 mode. The horizontal dashed black lines indicate the first and second resonance frequencies of the grooves (Fig. 2(a)), the former being the lowest asymptotic spoof plasmon frequency. (b.) Dispersion diagram of the SIS structure in Fig. 1(c) as calculated by Eq. (7i) (blue lines) and Eq. (7ii) (red lines), and finite element eigenfrequency analysis (circles). The geometrical parameters are the same as in (a). Points calculated by using by the self consistency condition of Eq. (1) using the reflection phase ϕ given by Eq. (4) overlap exactly with those obtained by Eqs. (3i) and (3ii), so they are not plotted. The dispersion curves of the unpatterned parallel plate waveguide (Fig. 1(a)) as well as the local cavity resonance frequencies (Fig. 2(a)) are indicated by dashed lines. Anticrossings occur when the parallel plate waveguide dispersion curves intersect the localized cavity resonance frequencies. Modes of opposite symmetries do not interact, so their dispersion curves can cross; for example, the lowest-frequency antisymmetric (red) mode does not share symmetry with the fundamental TEM mode of a parallel plate waveguide (blue, dashed), so a crossing occurs. (c.) Dispersion diagram of a gold SIS structure with the same geometrical parameters as in (b) calculated by finite element analysis, with material dispersion and losses taken into account (d.) Zoom in on the low frequency bands for a PEC SIS structure for gaps g = 10μm (solid lines) and 50μm (dashed lines) and a = 5μm, d = 10μm, and h = 50μm. The light line and the groove resonance frequency are shown in dotted black lines. The single surface SSP dispersion is shown by the dashed black line. The antisymmetric (red) mode becomes very flat for small gaps g. Inset: magnetic field distributions of approximately one period of the symmetric and antisymmetric modes for the points in the dispersion indicated by circular markers. The charge distribution on the two metallic surfaces has the opposite symmetry compared to that of the magnetic fields.

#147908 - $15.00 USD Received 23 May 2011; revised 25 Jun 2011; accepted 26 Jun 2011; published 18 Jul 2011

In the above discussion, we used the plane wave self consistency condition of Eq. (1) to determine the modes of the parallel plate waveguide of Fig. 1(a), and the transfer matrix method (Eqs. (2) and (3)) to determine the modes of the single corrugated interface of Fig. 1(b). Both of these approaches can be used to analyze the SIS waveguide, the basic geometry of which is shown in Fig. 1(c). Two metallic surfaces are separated by an air gap *g* and periodically corrugated with grooves of width *a*, period *d*, and height *h*. As for the single corrugated surface, the subwavelength corrugation is equivalent to a continuous PEC for TE polarized light, so we will only be analyzing the nontrivial TM case.

To apply the transfer matrix formalism, the SIS geometry can be viewed as a 6-layer system as shown in Fig. 1(c), and the matrices describing the system can be written down from Eqs. (2) and (3). Though we used this method to obtain the dispersion relation for the single corrugated interface of Fig. 1(b), it is not immediately apparent that calculating the reflection coefficient from the SIS structure using transfer matrices provides any information about the guided modes between the PEC slabs because the continuous PEC of layer 2 blocks all fields from entering the waveguide. The existence of layer 2 ensures that the reflection coefficient is identically −1, so it must hold that $M_{2,1} = -M_{1,1}$. However, when the layers underneath the first PEC layer are included in the calculation of *M*, $M_{1,1}$ (as well as $M_{2,1}$) has a series of zeros corresponding to removable singularities in the reflectance, which are associated with the eigenmodes of the buried structure. Therefore, it is possible to extract the guided modes of the SIS structure via the transfer matrix formalism.

We calculate the transfer matrix describing this system as $M = D_{12}\Phi_2 D_{23}\Phi_3 D_{34}\Phi_4 D_{45}\Phi_5 D_{56}$. By defining $r_{23} = -r_{32} = 1$, the wave vector inside the PEC region $k_{z,2}$ is cancelled out in the derivation. Note that $k_{z,2}$ is undefined, since no waves can propagate through a PEC. The condition $M_{1,1}$ yields the dispersion relation of the SIS structure that can be written as

$$1 = \frac{k_0}{\sqrt{\beta^2 - k_0^2}} \frac{a}{d} \tan(k_0 h) \left[\frac{\frac{\sqrt{\beta^2 - k_0^2}}{k_0} - \frac{a}{d}\tanh(g\sqrt{\beta^2 - k_0^2})\tan(k_0 h)}{\frac{\sqrt{\beta^2 - k_0^2}}{k_0}\tanh(g\sqrt{\beta^2 - k_0^2}) - \frac{a}{d}\tan(k_0 h)} \right] \qquad (6)$$

where β is the mode propagation constant and k_0 is the free space wave vector.

In Fig. 3(b), we plot the dispersion relation for a representative SIS structure designed to operate in the THz regime, where spoof plasmonic structures have been previously experimentally realized [10,16]. The geometric parameters are $a = 1\mu$m, $d = 10\mu$m, $h = 50\mu$m, $g = 50\mu$m. The range of plotted propagation constants β is significantly below the Brillouin zone boundary at $\beta_{BZ} = \pi / d$, ensuring the validity of the metamaterial limit and Eq. (6). Solid lines indicate the analytically calculated dispersion, while the circles represent points calculated by eigenfrequency analysis using the finite element method [36]. The analytical calculation and finite element analysis yield nearly identical results, verifying our derivation.

Due to the reflection symmetry of the waveguide structure about the x-axis, the modes possess either a symmetric (blue) or antisymmetric (red) character, with the symmetry in terms of the magnetic field with respect to the waveguide axis. The distribution of charges induced on the metallic surfaces possesses the opposite symmetry compared to that of the magnetic fields.

The SIS modes can be analytically separated according to their symmetry by using the transfer matrix method to calculate the reflection from two complementary structures, which comprise a corrugated layer, an air gap of thickness $g/2$, and a flat layer comprised of either (i) a PEC or (ii) a fictitious infinitely broadband PMC, with the PEC or PMC boundary conditions imposed at the axis of symmetry of the structure, shown as the grey dashed line in

#147908 - $15.00 USD Received 23 May 2011; revised 25 Jun 2011; accepted 26 Jun 2011; published 18 Jul 2011

Fig. 1(c). The antisymmetric modes of the SIS waveguide have an electric field node on the axis of symmetry, and therefore remain unchanged if the axis is replaced by a PEC boundary condition; likewise, the symmetric modes have an anti-node on the same axis, so a PMC boundary condition is used to isolate these modes. Applying this analysis yields the symmetric (i) and antisymmetric (ii) modes of the SIS waveguide:

$$\frac{\sqrt{\beta^2 - k_0^2}}{k_0} \tanh\left(\frac{g}{2}\sqrt{\beta^2 - k_0^2}\right) = \frac{a}{d}\tan(k_0 h) \tag{7i}$$

$$\frac{\sqrt{\beta^2 - k_0^2}}{k_0} \coth\left(\frac{g}{2}\sqrt{\beta^2 - k_0^2}\right) = \frac{a}{d}\tan(k_0 h) \tag{7ii}$$

Eqs. (7i) and (7ii) both correspond to Eq. (14) of [14] in the limit of $g \to \infty$, recovering the single surface SSP dispersion, and also to the non-corrugated parallel plate waveguide dispersion relation in the limit of $h \to 0$. Eq. (7ii) is also equivalent to Eq. (1) of [21] in the long-wavelength limit.

As in the case of the parallel plate waveguide, the SIS modes can be viewed as the combination of plane waves reflecting from the corrugated walls at some angle θ. The phase front self-consistency condition of Eq. (1) applies to the SIS waveguide, with the phase of reflection ϕ given by Eq. (4) and plotted in Fig. 2(b). This analysis breaks down for non-real angle θ $(\beta > k_0)$, so it can only capture the waveguide modes above the light line. We calculated the dispersion points above the light line by using this approach and found that the results match exactly with those obtained by the transfer matrix method (Fig. 3(b)).

The dispersion diagram in Fig. 3(b) can be understood in terms of the coupling between the modes of a parallel plate waveguide (dashed blue and red lines in Figs. 3(a) and 3(b)) and the localized cavity resonances of the grooves making up the SIS structure. The first and second order groove resonance frequencies (at $f_1 = c/4h$ and $f_2 = c/2h$) are plotted as horizontal dashed lines in Figs. 3(a) and 3(b). A single unit cell of the SIS structure consists of two counter-facing grooves separated by a gap g (shown by the dashed lines in Fig. 1(c)). The close proximity of the grooves hybridizes the modes of the grooves, creating a symmetric and antisymmetric mode, similar to the bonding and anti-bonding states of coupled quantum wells. These localized modes interact with the propagating modes of a conventional parallel plate waveguide, with some interactions disallowed by symmetry selection rules. At a point in wave vector - frequency space where a symmetric parallel plate waveguide mode (e.g. the fundamental TEM mode which follows the light line in Fig. 3) intersects a symmetric localized cavity mode, an anticrossing occurs. The same is true for antisymmetric modes, such as the TM1 waveguide mode (dashed red line in Figs. 3(a) and 3(b)) upon intersection with an antisymmetric cavity mode. This coupled mode behavior in the SIS waveguide is similar in character to the hybrid SSP/dielectric waveguide modes which have recently been investigated [37]. We performed finite element simulations to show that this behavior persists when gold is used instead of a PEC (Fig. 3(c)), with Drude parameters taken from Ref [38]. Note that the groove resonance frequencies are lower for a gold structure than one made from a PEC with the same geometric parameters, and the strength of the higher frequency anticrossings is smaller due to increasing waveguide losses at higher frequencies.

The modes below the light line in Figs. 3(b)–3(d) can also be viewed as the result of the evanescent coupling between SSP modes on each interface, in close analogy to the modes of a conventional MIM waveguide. In the MIM waveguide case, the symmetric and antisymmetric modes arise due to the coupling of surface plasmon modes on the two metal/dielectric interfaces [24, 39]. In the case of the SIS waveguide, the spoof plasmon modes due to the corrugations on the walls are likewise coupled to create two hybrid modes of opposite symmetries. Such modes have been previously observed in full-wave simulations both in the

#147908 - $15.00 USD Received 23 May 2011; revised 25 Jun 2011; accepted 26 Jun 2011; published 18 Jul 2011

metamaterial limit ($\lambda_0 >> d$) and away from it [18–20]. Representative magnetic field profiles for the symmetric and antisymmetric modes are shown in the inset of Fig. 3(d).

3. Applications of SIS Waveguides

As the gap g and duty cycle a/d decrease, the corrugation-enabled antisymmetric bands become extremely flat (e.g. solid red curve in Fig. 3(d)). Since the group velocity is defined as $v_{gr} = \partial\omega/\partial\beta$, flat bands correspond to very slow light, for which numerous applications have been identified [40]. The flat band in Fig. 3(d) is analogous to the 'omni-directional resonance' previously observed in MIM waveguides [41], which becomes progressively flatter as g→0, instead of only existing for a particular value of g as in MIM waveguides. Furthermore, the spectral position of this omnidirectional resonance given by the SIS structure can be engineered by varying the groove depth h.

The extensive control over mode dispersion provided by tuning the many degrees of freedom of the SIS waveguide enables the design of structures with multiple applications. In addition to the above slow light and 'omnidirectional resonance' configuration, by adiabatically tapering the parameters h, g, and a/d one can achieve the trapping (similar to Refs [42,43].) and super concentration (such as Ref. [44]) of light. Furthermore, one can envision dynamically changing the group velocity in the SIS waveguide by mechanically adjusting the gap g, creating a tunable delay line.

As a demonstration of the power of dispersion engineering in SIS waveguides, we propose a SIS waveguide with tapered groove depth h as a device to convert photonic modes into plasmonic ones, and the converse. The mode converter is illustrated in Fig. 4(a) and 4(b) and consists of three sections: the leftmost and rightmost sections are SIS waveguides with a = 5μm, d = 10μm, and g = 50μm and two different values of h (30μm and 60μm, respectively), while the middle is an adiabatically tapered SIS waveguide with h increasing linearly from left to right. The dispersion relation for one of the symmetric branches of a SIS waveguide with these geometric parameters is shown in Fig. 4(c) for a set of groove heights h from 30μm to 60μm.

Light is injected into the left port of the mode converter (h = 30μm) with an operating frequency of 3 THz (black dotted line in Fig. 4(c)). At this value of h, the dispersion curve lies above the light line (solid blue line in Fig. 4(c)), so $\beta < k_0$ and the mode can be called photonic. The magnetic field profile is shown in Fig. 4(a). As light passes through the middle part of the mode converter and enters the right part, h is gradually increased to 60μm, at which point $\beta > k_0$ and the mode becomes plasmonic (blue dashed line in Fig. 4(c)). The power flow diagram in Fig. 4(b) clearly shows that when the mode is photonic in character, the majority of the power flows through the middle of the waveguide, but when the mode becomes plasmonic, the power flow becomes localized around the edges of the waveguide. This photonic-plasmonic converter operates in an identical fashion in reverse: light injected into a plasmonic mode from the right port is converted into a photonic mode on the output.

#147908 - $15.00 USD Received 23 May 2011; revised 25 Jun 2011; accepted 26 Jun 2011; published 18 Jul 2011

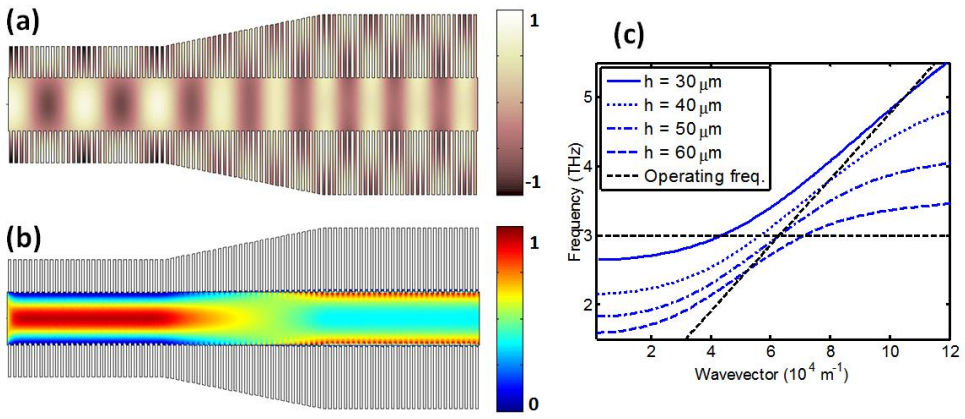

Fig. 4. (a.) Normalized magnetic fields in an SIS photonic-plasmonic mode converter calculated by the finite element method when a symmetric mode is injected from the left. (b.) The relative magnitude of the power flow in the mode converter. In the photonic mode on the left side, the majority of the power is flowing through the center of the waveguide, whereas in the plasmonic mode on the right side, the power flow is confined to the edges of the waveguide (c.) Dispersion diagram of an SIS waveguide with a = 5μm, d = 10μm, and g = 50μm for different values of h. The operating frequency of the mode converter is indicated by the horizontal dotted black line and the light line is indicated by the diagonal dashed black line.

While implementations of the SIS structures proposed here could be difficult to fabricate due to the ~λ/4 requirement for the groove height h coupled with the deep-subwavelength limit required for a and d (a,$d \ll \lambda$), other geometries are possible for which we expect similar dispersion to exist. It has been shown that nearly-planar geometries involving a metallic back-plane, a thin dielectric spacer, and metallic structures on top can support SSP modes [45, 46] and can function as artificial narrowband PMC surfaces (e.g. [29–31]). It is likely that these geometries can be used in the place of vertical grooves to create SIS waveguides which would be significantly easier to fabricate using conventional techniques.

4. Conclusion

We have analyzed the photonic and plasmonic modes of doubly-corrugated parallel plate structures which we refer to as spoof-insulator-spoof (SIS) waveguides. We analytically derived the dispersion relations of these modes in the limit of deeply-subwavelength corrugation, and found that they can be viewed as the interaction between the modes of a conventional parallel plate waveguide and hybridized localized cavity resonances of the grooves that make up the SIS structure. We found that the existence of this coupling, which is indicated by anticrossings in the dispersion curves, is dependent on symmetry-based selection rules. We anticipate that these SIS structures will be useful as waveguides in the mid-IR, THz, and RF regimes due to the extensive range of tunability in their dispersion curves provided by the many geometrical degrees of freedom of the structures, enabling applications such as low-group-velocity delay lines and photonic-plasmonic mode converters.

Acknowledgments

We acknowledge funding from AFOSR under contract no. FA9550-09-0505-DOD. M. A. Kats is supported by the National Science Foundation through a Graduate Research Fellowship. We thank Jonathan Fan, Rashid Zia, and Alexey Belyanin for helpful discussions.

#147908 - $15.00 USD Received 23 May 2011; revised 25 Jun 2011; accepted 26 Jun 2011; published 18 Jul 2011